Journal of Applied Fluid Mechanics, Vol. 13, No. 6, pp. x-x, 2020.
Available online at www.jafmonline.net, ISSN 1735-3572, EISSN 1735-3645.
DOI: 10.36884/jafm.13.06.xxxxx

Performance Analysis of Flapping Foil Flow Energy Harvester Mounted on Piezoelectric Transducer using Meshfree Particle Method

M. Jamil[1], A. Javed[1†], S. I. A. Shah[1], M. Mansoor[1], A. Hameed[1] and K. Djidjeli[2]

[1]*College of Aeronautical Engineering, National University of Sciences and Technology, Islamabad, Pakistan*
[2]*University of Southampton, Southampton, UK*

†*Corresponding Author Email: ali.javed@cae.nust.edu.pk*

(Received December 28, 2019; accepted May 16, 2020)

ABSTRACT

Performance of a semi-active flapping foil flow energy harvester, coupled with a piezoelectric transducer has been analyzed in this work. The airfoil is mounted on a spring, damper and piezoelectric transducer arrangement in its translational mode. External excitation is imparted in pitch mode and system is allowed to oscillate in its translational mode as a result of unsteady fluid forces. A piezoelectric transducer is used as an electrical power converter. Flow around moving airfoil surface is solved on a meshfree nodal cloud using Radial Basis Function in Finite Difference Mode (RBF-FD). Fourth order Runge-Kutta Method is used for time marching solution of solid equations. Before the solution of complex Fluid-Structure Interaction problem, a parametric study is proposed to identify the values of kinematic, mechanical and geometric variables which could offer an improved energy harvesting performance. For this purpose, the problem is modelled as a coupled electromechanical system using Lagrange energy equations. Airfoil lift and pitching moment are formulated through Theodorson's two dimensional thin-plate model and a parametric analysis is conducted to work out the optimized values of pivot location, pitch amplitude, spring stiffness and damping constant. The subsequent computational analysis resulted in an enhanced performance compared to the potential flow model with an efficiency of up to 27% based on total power extraction through the flow. Higher efficiency is obtained when the pitch axis is located aft of mid chord. However, this setting does not correspond to the maximum power output. Interestingly, power is maximized at much lower efficiency values.

Keywords: Bio-inspired; Semi-active flapping foil; Electromechanical coupling; Dynamic stall effect.

NOMENCLATURE

a	non-dimensional distance of pivot point from mid-chord (chords)
b	semi-chord of foil
c	damper strength
C_p	capacitance of piezoelectric layer
$\bar{C}_{op}$	cycle-averaged power coefficient
$\bar{C}_{op(\text{flow})}$	cycle-averaged power coefficient based on power extracted through transducer and damper
$\bar{C}_{op(\text{electric})}$	cycle-averaged power coefficient based on power extracted through transducer.
d	vertical displacement of foil
f^*	non-dimensional frequency
h	heaving amplitude
k	spring constant
LEV	leading Edge Vortex
P_{piezo}	average power through piezoelectric transduction
P_{damp}	average power through damper idealized as generator
R	resistance of piezoelectric layer
Re	Reynolds number.
St	Strouhal number.
T	time period of oscillation
U	free stream velocity
V	voltage
α_{max}	maximum angle of attack amplitude
$\eta_{electric}$	efficiency based on net power output through piezoelectric transduction.
$\eta_{f\ low}$	efficiency due to net power extracted through transducer and damper.
θ_c	electromechanical coupling constant
θ_o	pitch amplitude
ρ	density of fluid
ω	forcing frequency

1. INTRODUCTION

Search for renewable energy resources and strategies is the prime technological and economic challenge in the present era. Past few years have seen an extensive focus on the utilization of hydro-power in the form of tidal and ocean currents as renewable energy source. The biomimetic studies have helped researchers gain a better insight about the mechanics and locomotion of various aquatic animals. In the same aspect, bio-inspired flapping foils have been scientifically investigated as potential energy harvesters such as studies undertaken by Triantafyllou *et al.* (2004). The flow induced flapping foils have been analyzed to produce high instantaneous forces due to dynamic stall effect such as Leading Edge Vortices (LEVs) and it is natural to consider them as an alternate energy source.

Flapping foil energy harvesters are governed by two degrees of freedom namely pitch and heave (plunge) motions. These are categorized into three main types based on the activating mechanism, where the pitching and plunging degrees of freedom have prescribed or free motions (Xiao and Zhu (2014)). Most of the studies have been focused on fully active systems such as work by Kinsey and Dumas (2008), Zhu (2011), Xiao *et al.* (2012), Wu *et al.* (2016) and Javed *et al.* (2018), which involve fully prescribed motions, where a known frequency and amplitude is imposed on both the pitching and heaving modes. Such a system will extract positive power from the flow when the measured time-averaged power input driving the motion is negative. However, such systems do not take into consideration the loads to which the system would be providing power or the periods when the sys-tem would be drawing negative output power. In semi-active systems such as work by Shimizu *et al.*(2008), Deng *et al.* (2015) and Javed *et al.* (2018), a prescribed frequency and amplitude is imparted to the pitching mode through a driving motor while power is extracted through the flow induced plunging motion. For such a system, a viscous damper is idealized as a load which is connected across the plunging motion. Net power output depends upon the difference between the input power of the motor and power extracted via a damper. For fully-passive systems (Qadri *et al.* (2019)), both heaving and pitching modes are induced by instabilities in the flow. Here parameters of the system such as frequency and amplitude for the oscillations are dictated by the flow-generated forces and vortex interactions, so the model is much more sensitive to flow conditions and numerical procedure applied for solution. Such systems are also analyzed while coupled with an attached load which is modelled as a viscous damper along with the heave mode.

Semi-active systems offer the most feasible configuration in practice so, earlier industrial prototypes have employed such configuration in their design. An example is of Stingray which was a 150kW power generator, extracting energy through a flapping foil energy harvesting systems (Finnigan (2012)). Later on, Zhu *et al.* (2009) modelled the capacity of a semi-active flow energy harvester by utilizing a 2D potential flow model. The study was of particular interest, as it had addressed the issue of how flapping foils extract power from the flow through a linear damper which is idealized as a generator, a study, which was not previously undertaken for such systems. An efficiency of 25%was achieved from the plunge motion based on optimum combination of frequency, pitch angle and damper strength. Zhu and Peng (2009) later utilized a viscous flow solver for a 2D Navier-Stokes model to examine the effects of LEV formation. According to their findings, net positive power out-put is strongly dependent upon LEV and there exists a range of pitching frequencies $k = 0.8 - 1.4$ for such power output. The LEV generates a low-pressure region which enhances the lifting forces, and subsequently output energy, while the viscous damping tends to reduce the energy harvesting capacity. It was also found out that a foil's pivot location is crucial in determining the balance of these two competing effects. Deng *et al.* (2015) numerically investigated the performance of a flapping foil energy harvester system in a semi-active configuration. They obtained a power output efficiency of 34% for their model at optimal values of dimensionless forcing frequency ($f^* = 0.16$), pitching amplitude ($\theta_o = 75^o$) and mass ratio $\mu = 1$.

Traditionally, literature for flapping foil energy harvesting systems is limited and such systems idealize viscous damper as a power extractor. However, the question still remains open that how can energy extracted through such energy harvesting systems be utilized for useful purpose through an electrical converter? Additionally, for commercial development of such systems, there is a need for formulation of extensive mathematical models incorporating the coupled effects of fluid-structure interaction, mechanical system efficiencies and consideration with regards to the type of electric converter. There can be various generators for conversion of mechanical to electrical energy among which piezoelectric transducer is one such converter which utilizes the mechanical energy to generate voltage. They offer certain advantages over various other electric converters including small size, rugged construction, high power output and higher frequency response where parameters varying at high speeds can be sensed easily. In this regard, various studies have been conducted in the recent past, to analyze the factors affecting energy harvesting through piezoaeroelastic systems. For example, Abdelkefi *et al.* (2012) analyzed the effects of structural nonlinearities such as torsional and flexural spring coefficients on the dynamic behaviour of a piezoaeroelastic system. It was found out that the non-linear torsional spring has the most influence on the onset of system's instability, while maximum power output corresponded to a specific value of electrical load resistance. Subsequent studies by Mehmood *et al.* (2013) on vortex induced oscillations of a circular cylinder coupled with a piezoelectric converter showed that, maximum harvested power is achieved at an optimum value of electrical load resistance. Interestingly, this maximum harvested power point did not correspond to maximum vibrational amplitudes of the cylinder.

Present study focuses on the investigation of energy harvesting from a semi-active foil system by utilizing a piezoelectric transducer. However, prior to solving the computationally intensive coupled Fluid-Structure Interaction problem, the values of system parameters, for achieving high energy harvesting efficiency, have been estimated by solving a relatively simpler linearized model of coupled electromechanical system. The fluid forces appearing in the rigid body motion equations are modelled using Theodorson's 2D thin-plate model. The behaviour of piezoelectric transducer is modelled by Gauss Law as suggested by Abdelkefi *et al*. (2012). By analyzing this system, we have been able to predict that how power extracted through a flapping foil system can be utilized for useful purpose through an electric converter. In this regard, present paper is arranged as follows. In Section 2., physical and mathematical model for the problem has been discussed along with the formulation of governing equations for harvester's performance indicators. In Section 3., analytical results have been depicted where optimization of various performance parameters is examined. Numerical simulations are discussed in Section 4., where the effect of dynamic stall on harvester's power extraction capability and corresponding efficiencies is reviewed. Finally, conclusion and direction for future course of study is presented in Section 5.

2. PROBLEM FORMULATION

2.1 Physical and Mathematical Model

A foil is considered with mass ~~m~~ and semi-chord length of *b*. The foil is mounted on a spring and damper system while it is subjected to uniform, in-compressible flow of velocity *U* as shown in Fig.1. The pivot point location *P* of foil is at a non-dimensional distance of *a* with reference to mid chord. A prescribed pitching motion is imposed upon the foil given as $\theta(t) = \theta_o e^{i\omega t}$ while heaving motion $y(t)$ is activated by flow-induced forces. Adding a piezoelectric transducer along the translational motion of foil and including a load resistance R in the electrical circuit, a coupled electromechanical system of equations is obtained as shown below:

$$m\ddot{y} + c\dot{y} + ky - \theta_c V = L \tag{1}$$

$$C_P\dot{V} + \frac{V}{R} + \theta_c\dot{y} = 0 \tag{2}$$

where *V* is the voltage generated across the load resistance, C_p represents the capacitance of piezo-electric layer and θ_c is the electromechanical coupling constant. Similar piezoelectric model is utilized by Abdelkefi *et al*. (2012) in their analysis of piezoaeroelastic energy extractors.

2.2 Hydrodynamic Force and Moment

The formulation of hydrodynamic lifting force and moment is based on Theodorsen's 2D thin-plate model (Hodges and Pierce 2011). The model can solve lift distribution around an idealized airfoil which is harmonically pitching and heaving in an inviscid, incompressible flow. The model also assumes small deflections for the flat plate, so flow ~~re-mains~~ attached and leaves an idealized planar wake. If the pitching and heaving motions are given as $\theta = \theta_o e^{i\omega t}$ and $y = y_o e^{i\omega t}$ respectively, then the hydrodynamic lift force is formulated as a sum of quasi-steady lift, added mass effects of displaced fluid and changes in induced circulation around an airfoil due to wake (Hodges and Pierce (2011) and Harper *et al*. (1998)) which gives

$$\begin{aligned} L = {} & 2\pi\rho bU\left(-y + U\theta + \left(\frac{b}{2} - a\right)\dot{\theta}\right)C(i\omega) \\ & + \rho\pi b^2\left(-\ddot{y} + U\dot{\theta} - a\ddot{\theta}\right) \end{aligned} \tag{3}$$

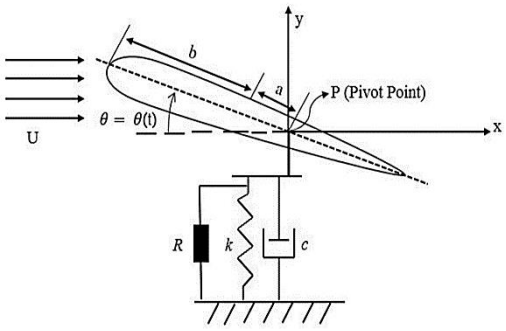

Fig. 1. Schematic for the model where *a* is the non-dimensional distance of pivot axis from mid-chord and b is the semi-chord length of foil.

Based on hydrodynamic lift, moment is formulated as:

$$\begin{aligned} M = {} & \frac{\pi\rho b^2 U}{4}\dot{\theta} + \frac{\pi\rho b^4}{8}\ddot{\theta} \\ & -\pi\rho b^2 U\left(-\dot{y} + U\theta + \left(\frac{b}{2} - a\right)\dot{\theta}\right)C(i\omega) - aL \end{aligned} \tag{4}$$

So net moment becomes

$$\begin{aligned} L = {} & -\pi\rho b^2[a(\ddot{y}) + \left(\frac{b}{2} - a\right)U\dot{\theta} + b^2\left(\frac{1}{8} + \frac{a^2}{b^2}\right)\ddot{\theta} \\ & - U\left(\frac{2a}{b} + 1\right)(-\dot{y} + U\theta \\ & + \left(\frac{b}{2} - a\right)\dot{\theta})C(i\omega)] \end{aligned} \tag{5}$$

Theodorsen's function $C(i\omega)$ accounts for the ~~ex-tent~~ of vortex shedding from the foil and is approximated by a ratio of third-order polynomial. Further details about the Theodorsen's function have been discussed in the work of Harper *et al*. (1998). The hydrodynamic moment M_h can be calculated from Eq.5 and is expressed as $M_h = M_o e^{i\omega t}$:

As the prescribed pitch motion, flow induced heave and generated voltage are given by a sinusoidal pro-file as $\theta = \theta_o e^{i\omega t}$, $y = y_o e^{i(\omega t)}$ and $V = V_o e^{i(\omega t)}$ respectively then using Eq.3, Eq.1 and Eq.2 simplify

to:

$$\left(-\omega^2 M_t + Di\omega + k\right)y_0 - \theta_c V_0 = F_0, \quad (6)$$

$$\theta_c i\omega y_0 + \left(C_p i\omega + \frac{1}{R}\right)V_0 = 0, \quad (7)$$

where $M_t = m + \rho\pi b^2$, $D = c + 2\pi\rho bUC(\sigma)$ and $F_0 = \left[2\pi\rho bU^2 + 2\pi\rho b^2 U\left(\frac{1}{2} - a\right)(i\omega)\right]C(\sigma) + \rho\pi b^2 U(i\omega) + \rho\pi b^2 a\omega^2$

which can be written in matrix form as

$$\begin{bmatrix} -\omega^2 M_t + k + i\omega D & -\theta_c \\ \theta_c i\omega & \frac{1}{R} + iC_p\omega \end{bmatrix}\begin{bmatrix} y_0 \\ V_0 \end{bmatrix} = \begin{bmatrix} F_0 \\ 0 \end{bmatrix} \quad (8)$$

So the net mass M_t and damping D incorporate the effect of displaced fluid mass and hydrodynamic damping which can be used to calculate the heaving amplitude and generated voltage due to piezoelectric effect through Eq.8 as $h = |y_o|$ and $V_{piezo} = |V_o|$ respectively. Furthermore, the heaving amplitude h and voltage V_{piezo} along with the induced hydrodynamic moment are utilized to estimate the performance indicators for our energy harvester which are formulated below.

2.3 Performance Parameters

Performance of a flapping foil energy harvester is measured in terms of net power output and efficiency. For the problem in hand these parameters are defined as follows:

2.3.1 Power Input

The average power input to activate the pitching motion is expressed as $P_{input} = M_{actuator}\dot{\theta}$. If rotational inertia of foil is neglected then $M_{actuator} + M_h = 0$ or $M_{actuator} = -M_h$. So the cycle-avera d input power can be found as $P_{input} = \frac{1}{T}\int_0^T -M_h\dot{\theta}d(t)$. As $M_h = M_o e^{i\omega t}$, then average input power becomes:

$$P_{input} = \frac{-\theta_0\omega\,\mathrm{Im}(M_0)}{2} \quad (9)$$

where (*Im*) depicts the imaginary part of M_o

2.3.2 Power Output

For a simple flapping foil system with no electromechanical coupling, the power extracted from flow is idealized through a damper (Xiao and Zhu (2014)). So, in the present case if damper is also idealized as generator, then average power generated through the linear damper with strength c is given as P_{damp} and is calculated as:

$$P_{damp} = \overline{c\dot{y}^2} \quad (10)$$

The cycle-averaged power output is expressed as $P_{damp} = \frac{1}{T}\int_{t_0}^{t_0+T} c\dot{y}^2 d(t)$ where T is time period given as as $T = \frac{2\pi}{\omega}$. The Eq.10 then becomes:

$$P_{damp} = \frac{ch^2\omega}{2} \quad (11)$$

However, for a coupled electromechanical system, power extraction is not so simple and depends upon various other factors including damper strength and piezoelectric resistivity. The average power extracted through the piezoelectric transduction can be calculated as:

$$P_{piezo} = \frac{V_{piezo}^2}{R} \quad (12)$$

2.3.3 Net Power Output

Net power output is described in two ways. Useful power is the net electric power that is extracted through flow via piezoelectric transducer. We denote it by $P_{net(electric)}$ and is given at Eq.13:

$$P_{net(electric)} = P_{piezo} - P_{input} \quad (13)$$

However, if we assume both damper and piezoelectric transducer as an idealized electric generator, then it would give an estimation of gross energy that is extracted through the flapping foil energy harvester. We denote it as $P_{net(flow)}$ and is given at Eq.14:

$$P_{net(flow)} = \left(P_{piezo} + P_{damp}\right) - P_{input} \quad (14)$$

Certainly useful energy extracted via transducer can still be enhanced at the expense of power output idealized through the damper.

2.3.4 Efficiency

Efficiency of the harvester is defined as the ratio between net power extracted to the power available in the incoming flow (Kinsey and Dumas (2014)). So, efficiencies for respective types of power output are calculated as follows:

1. Efficiency due to net power output through piezoelectric transduction is:

$$\eta_{electric} = \frac{P_{net(electric)}}{\frac{1}{2}\rho U^3(2h)} = \frac{P_{net}}{\rho U^3 h} \quad (15)$$

where *2h* denotes twice the amplitude of heaving motion as given by Kinsey and Dumas (2014) .

2. Similarly, efficiency due to net power extracted through transducer as well as the damper is calculated as:

$$\eta_{flow} = \frac{P_{net(flow)}}{\rho U^3 h} \quad (16)$$

3. ANALYSIS OF MATHEMATICAL MODEL AND RESULTS

Performance analysis is based on key factors that effect the power outputs and efficiencies of a flow

energy harvester. They mostly comprise of kinematic, geometric and structural parameters as dis-cussed below:

3.1 Effects of Geometric and Structural Parameters

So, the structural parameters (stiffness and damping) as well as piezoelectric parameters (external load and capacitance) need to be optimized for achieving the best performance. Studies have shown that structural stiffness and damping strength along with the location of pitch axis greatly effect the performance of a flapping foil energy harvester (Zhu *et al.* (2009)). Similarly, as discussed by Xiao and Zhu (2014), the maximum net power output of a harvester always depends upon the damper with a particular strength. So, the value of damping strength should be tuned according to the flow conditions for maximizing power extraction. Zhu and Peng (2009) while discussing results for their 2D model had predicted a maximum theoretical power extraction for a semi-active flap-ping foil energy harvester. This value is valid at any value of pitching axis and structural stiffness provided it is subjected to harmonic motion at low forcing frequency. Same equation is reproduced at Eq.17, based on our model's parameters. Further, this maximum power is achieved at a damping coefficient of ($c = 2\pi\rho bU$) which clearly depends upon the flow field velocity.

$$P_{max} = \frac{\pi}{4}\rho b U^3 (\theta_0)^2 \qquad (17)$$

(a) Leading edge (a = -0.5)

(b) $\frac{1}{4}$ of chord (a = -0.25)

(c) $\frac{1}{3}$ of chord (a = -0.16)

(d) Mid chord (a = 0)

(e) $\frac{3}{4}$ of chord (a = 0.25)

(f) Trailing edge (a = 0:5)

A parametric study has been carried out to obtain the zones of maximum performance for our energy harvester similar to the potential flow analysis by Zhu and Peng (2009) and Jamil and Javed (2019). Various isolines have been acquired for net power output $P_{net(flow)}$ and efficiency η_{flow} at six distinct pivot locations as depicted at Fig.2 and Fig.3. The figures are obtained at different combinations of damping coefficient (c) and forcing frequency (ω) while the pivot locations correspond to non-dimentionalised distance a=−0.5, −0.16, −0.25, 0,0.25, 0.5 measured from the mid-chord of foil. For ease of calculations, flow parameters density(ρ), velocity(U) and chord length ($2b$) have all been assumed to be unity while the structural stiffness is taken as zero with pitching amplitude of $\theta_o = 10^o$ unless stated otherwise. Moreover, as the mass of foil is negligible com-pared to fluid added mass, so it is ignored. For piezoelectric transducer the factors including coupling constant θ_c, capacitance C_p and resistance R determine the generation of electric power P_{piezo}. For calculation, coupling constant θ_c and capacitance C_p have been non-dimentionalised as 1 while an optimize value for resistance $R_{opt} = \frac{1}{\omega C_p}$ is adopted which depends upon the capacitance of the transducer as well as the forcing frequency (Chin *et al.* (2017)). The net power output $P_{net(flow)}$ is non-dimentionalised with respect to maximum out-put power depicted at Eq.17. Following key observations have been made from parametric isolines depicted at Fig.2 and 3:

- When pitch axis is located at of 1/3 chord (a =−0.16, Fig. 2(c) and 3(c)), maximum power $P_{net(flow)}$ = 0.8 is obtained at low frequencies ω < 1. However, efficiency is maximized (η_{flow} = 8%) within the range ω 1−2.5 and it corresponds to net power output of $P_{net(flow)}$ = 0.6 − 0.4. The behavior of system is similar when pitch axis is at quarter chord (a = −0.25). However, numerical values of parameters are different as can be seen from Fig. 2(b) and 3(b)

- The power output tends to increase as the pitch axis move forward and maximized when a =−0.5 (pitch axis at leading edge, Fig. 2(a) and 3(a)). However, the efficiency tends to re-duce by moving the pitch axis forward. At a = −0.5, maximum power output reaches $P_{net(flow)}$ = 0.8 whereas the efficiency remains in the range η_{flow} = 3 − 6%.

- When pitch axis is at mid-chord (a = 0, Fig. 2(d) and 3(d)), maximum efficiency of η_{flow} = 9% is obtained at ω 1−2 with corresponding power extraction of $P_{net(flow)}$ = 0.8 − 0.4.

- When pitch axis is located at 43 of chord length (a = 0.25, Fig. 2(e) and 3(e)), positive power output is achieved at low forcing frequencies (ω ≤ 1). However, efficiency keep on increasing with an increase in frequency and damping, and it may even go beyond 1 at high values of frequency and damping. Such a peculiarity is due to the exclusion of pitching motion in the efficiency formulation. The results also depict that net power output de-creases with increasing frequency and damping, and it may even become zero at higher values. Such results at 3/4 of chord length are spurious and have not been considered for further analysis.

- The zone of maximum efficiency moves closer to the zone of maximum power when the pitch axis is located at trailing edge as shown in Fig. 2(f) and Fig. 3(f)). Therefore, the possibility of achieving maximum power with higher efficiency increases at such an arrangement.

Among the cases discussed earlier, superior energy harvesting performance is achieved at the pitch axis location of mid chord with maximum power extraction efficiencies of η_{flow} = 9% and corresponding maximum power output coefficients of $P_{net(flow)}$ = 0.8, within the range of forcing frequency and optimal damping strength considered. Further simulations were carried out at pitch axis location of mid-chord with stiffness k = 10. The zones for positive power extraction become narrower

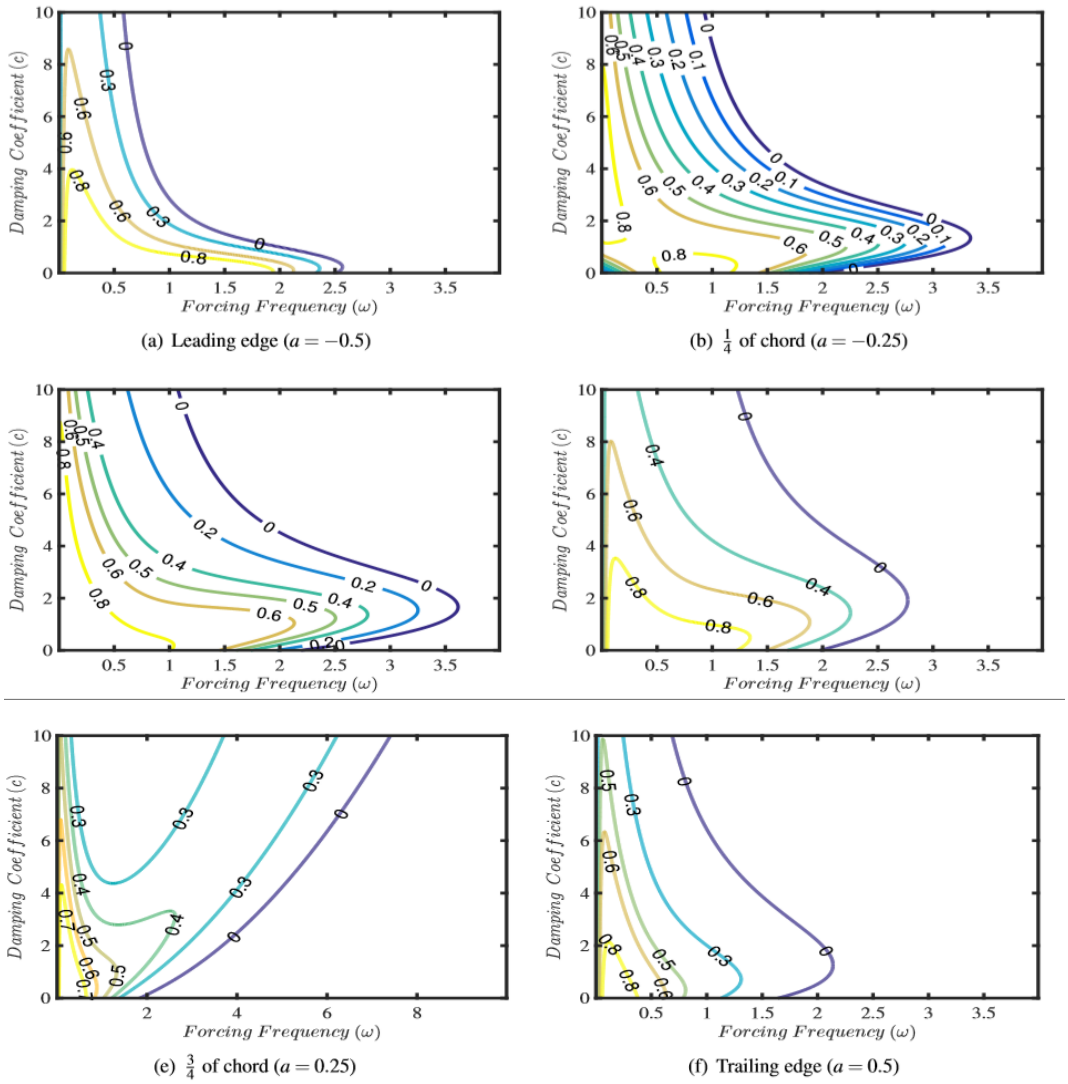

Fig. 2. Isolines for net power $P_{net(flow)}/P_{max}$ calculated at six different pitch axis locations (a =−0.5,−0.25,−0.16,0,0.25,0.5) and as a function of forcing frequencies (ω) and damping coefficient (c).

and eventually vanish at higher values of k, c and ω. In view of the discussion, best performance is possible when the pitch axis is kept at mid-chord (a = 0) and structural stiffness is kept minimal at (k=0).

The net power efficiencies η_{flow} through flow at all the selected pivot location as shown in Fig.2 and 3 are low, however, they provide the feasibility of employing coupled electromechanical flapping foil systems as energy harvesters. Similar analysis based on potential flow model by Zhu and Peng (2009) has also predicted such low efficiencies for a simple flapping foil energy harvester system.

~~(a) Heave (h) and voltage (V_{piezo}) as a function of pitch amplitude~~

~~(b) $P_{net(\ f\_low)}$ and $P_{net(electric)}$ as a function of pitch amplitude~~

~~(c) $h_{f\ low}$ and $h_{electric}$ as a function of pitch amplitude~~

3.2 Effect of Pitch Amplitude

Effect of varying pitch amplitude shows that heaving amplitude, generated voltage (Fig. 4(a)) and power output efficiencies (Fig. 4(c)) vary linearly with increasing pitch amplitude. However, net power output varies non-linearly with increasing pitch amplitude (θ^o) as shown at Fig. 4(b). Such behaviour is also evident from the power and efficiency formulation. Results at Fig.4 necessitate a threshold limit for the pitch amplitude, where the basic assumptions for Theodorsen's thin plate model of small-amplitudes motion and attached flow may not be violated. Moreover, high pitch amplitudes also give rise to LEVs as depicted by Zhu and Peng (2009), which would violate the potential flow analysis.

Previous studies such as work conducted by Anderson *et al.* (1998) had shown that factors including Strouhal number (St) and effective AoA (α_{max}) affect the flow separation and formation of LEVs. Through an experimental study, they found out that for St< 0.12 and αmax < 20^o, with accompanying heaving amplitude of the order of

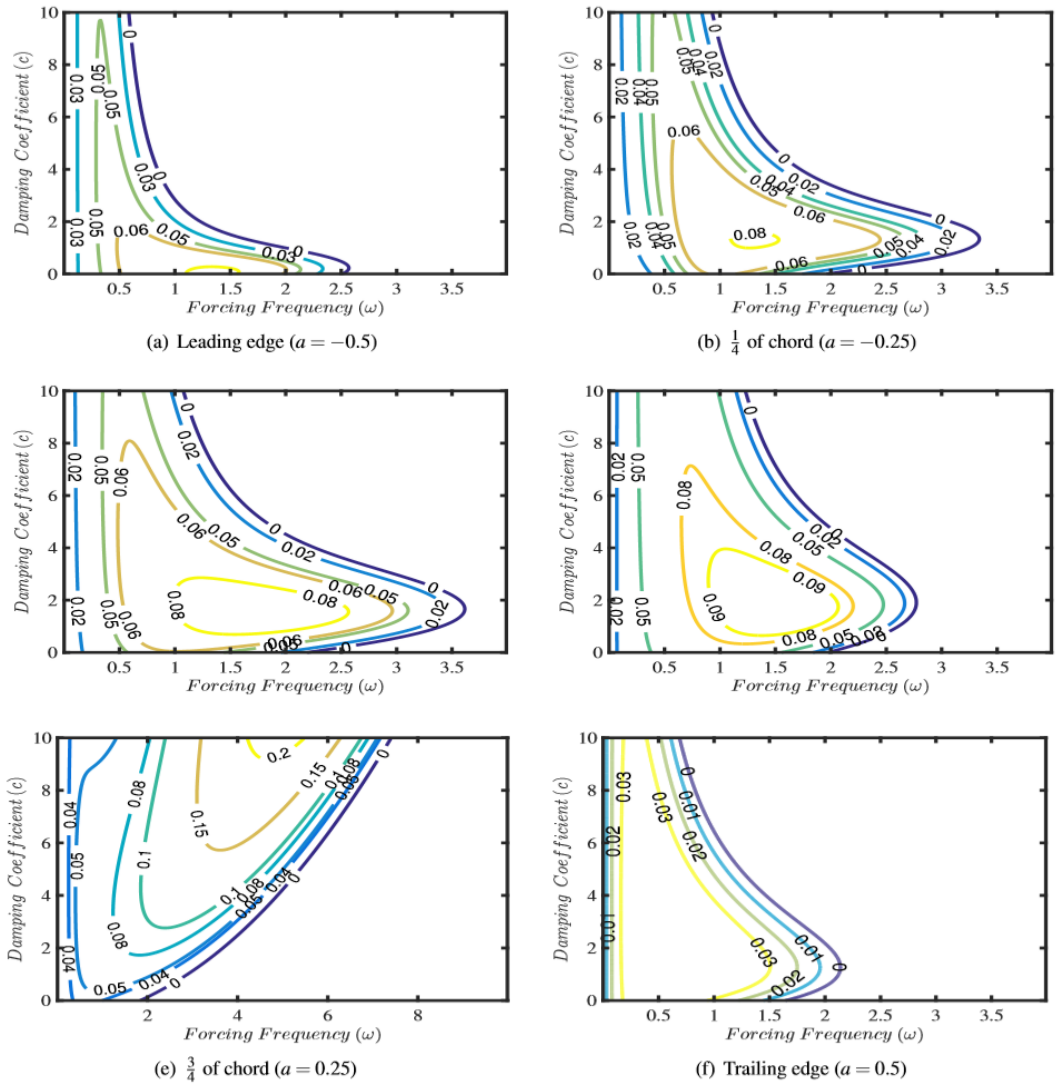

(a) Leading edge ($a = -0.5$)

(b) $\frac{1}{4}$ of chord ($a = -0.25$)

(e) $\frac{3}{4}$ of chord ($a = 0.25$)

(f) Trailing edge ($a = 0.5$)

Fig. 3. Isolines for efficiency η_{flow} calculated at six different pitch axis locations (a = −0.5,−0.25,−0.16,0,0.25,0.5) and as a function of forcing frequencies (ω) and damping coefficient (c).

$\frac{h}{2b} \approx 1$, the effect of LEVs can be neglected. When the present problem is analyzed, it was found that below the pitch amplitude of $\theta_o = 20^o$, the St and αmax remain below the limiting factors of 0.12 and 20^o respectively. So, the optimal pitch amplitude θ_o that can be adopted for further studies without violating the potential flow assumption is 20^o.

3.3 Optimal Power and Frequencies

The simulations at Fig.5 conducted at pitch axis location of mid-chord and limiting case of spring stiffness ($k = 0$), depict that high heaving amplitudes, voltages and net power outputs are obtained at low forcing frequencies and decrease with increasing forcing frequencies. However, corresponding efficiencies are lower at low forcing frequencies. Such behaviour was also predicted by Shimizu *et al.* (2008) who achieved high efficiencies only at low heaving amplitudes and high forcing frequencies. Physically, this can be attributed to the fact, that due to low structural stiffness, natural frequency of the system will be lower. So low forcing frequencies can induce corresponding high heaving motion due to resonance.

Figure 5(b) depicts that maximum net power generated through transducer($P_{net(electric)}$) is 0.63 at ω 1 while maximum net power extracted through the flow ($P_{net(flow)}$) is 0.82 around ω 0.14 . Similarly, Fig.5(c) shows that maximum net electric power efficiency ($\eta_{electric}$) is around 5% while positive efficiencies have been predicted when ω < 0.8. The net efficiency for total power extracted through the flow (η_{flow}) is 16%, which is three times higher than that generated via the transducer.

The efficiencies are low as they have been calculated based on the Theodorsen's 2D thin plate theory which assumes linear, small-amplitude, low-frequency motions. The theory also assumes

potential flow where flow remains attached and negates the effects of LEVs. So, it is important that the dynamic stall effects may be taken into consideration for realistic estimation of power generation efficiencies which has been done in Section 4.

~~(a) Heave and voltage as a function of frequency~~

~~(b) P_{net}/P_{max} as a function of frequency~~

~~(c) Efficiency as a function of frequency~~

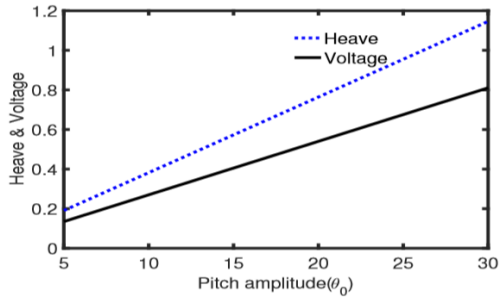

(a) Heave (h) and voltage (V_{piezo}) as a function of pitch amplitude

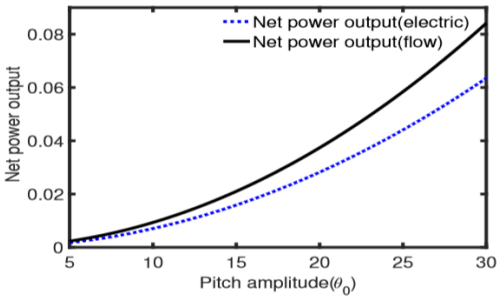

(b) $P_{net(flow)}$ and $P_{net(electric)}$ as a function of pitch amplitude

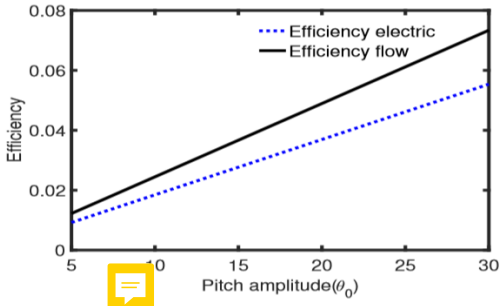

(c) η_{flow} and$\eta_{electric}$ as a function of pitch amplitude

Fig. 4. Calculated relation of heaving (h) amplitude, voltage (V) amplitude, net power outputs and efficiencies with pitch amplitude, where pitch axis is at mid-chord (a = 0) , k = 0 and $c = \pi$. Pitch amplitude of $\theta_o = 20^o$ can be adopted as the optimum value where potential flow assumption of Theodorsen's thin-plate theory is not violated.

4. NUMERICAL SOLUTION

Analytical results calculated at Section 3. are based on Theodorsen's 2D thin-plate model. The model assumes potential flow where dynamic stall effects are ignored. Leading edge vortices (LEVs) are a prominent outcome of dynamic stall effect and are considered a prime factor for the generation of lift which enables insects to hover and move forward during flight (Shyy *et al.* (2010)). Dynamic stall effects can be modelled by numerically solving the Navier-Stokes equation. For this purpose, an in-house algorithm presented by Javed *et al.* (2016) is utilized to model the coupled electromechanical semi-active flapping foil system and estimate the lift/moment forces based on the governing equations formulated at Section 2.

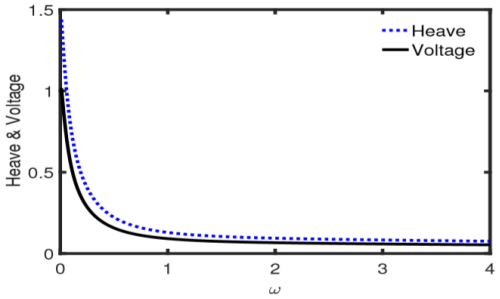

(a) Heave and voltage as a function of frequency

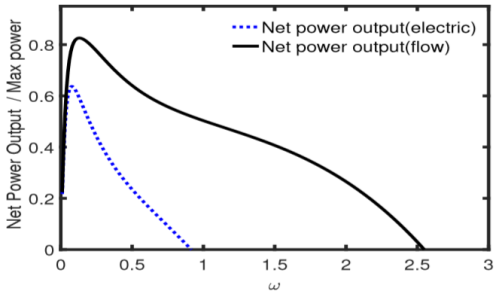

(b) P_{net}/P_{max} as a function of frequency

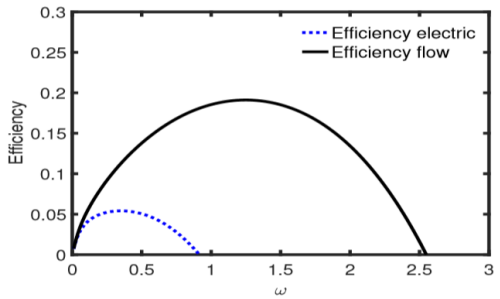

(c) Efficiency as a function of frequency

Fig. 5. Calculated relation of heaving (h) amplitude, voltage (V) amplitude, net power outputs and efficiencies with forcing frequency(ω) where pitch axis is located at mid-chord (a = 0) , k = 0 and $c = \pi$. Relatively high heaving amplitudes, volt-ages and net power outputs are obtained at low forcing frequencies. Maximum net efficiency for total power extracted through the flow (η_{flow}) is 16%.

4.1 Hybrid Fluid Solver

The scheme utilizes a body conformal meshfree

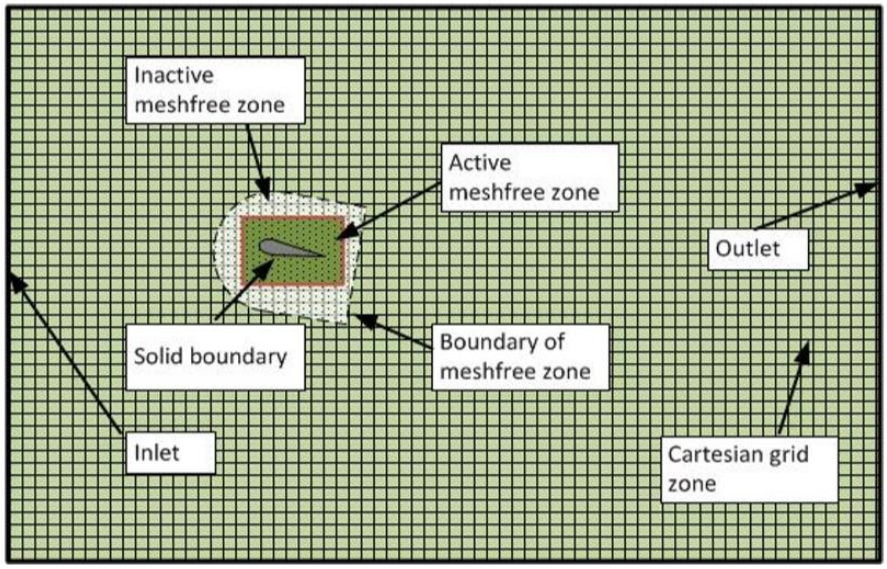

Fig. 6. Meshfree-Cartesian Hybrid grid scheme by Javed *et al.* (2016).The scheme utilizes a body conformal meshfree nodal region around the foil in the near field and a static Cartesian mesh in the far region which partially overlaps the meshfree region. .

nodal region around the foil in the near field and a static cartesian mesh in the far region which partially overlaps the meshfree region. In this way a hybrid grid is formed as shown in Fig.6. The flow equations over dynamic meshfree zone are solved with Arbitrary Lagrangian Eulerian (ALE) frame. With Ω_0 as the initial configuration of computational domain at time t_0 , it can be mapped over current configuration Ω_t at any arbitrary time t as:

$$A:\Omega_0 \rightarrow \Omega_t \tag{18}$$

$$X \rightarrow x(X,t) = A_t(X) \tag{19}$$

ALE velocity is calculated as $\vec{v} = \partial A_t / \partial t$. At each node, ALE velocity is set equal to the velocity of node. Non-dimensionalized pressure-velocity ($\vec{P}, \vec{u}$) form of time varying, incompressible, viscous flow equations in ALE formulation is given as (Takashi and Hughes (1992)):

$$\partial_t \vec{u} = -\nabla P - (\vec{u} - \vec{v})).(\nabla \vec{u}) \_ (1/\mathrm{Re})\nabla^2 \vec{u} \tag{20}$$

$$\nabla.\vec{u} = 0 \tag{21}$$

At each node, ALE velocity is set equal to the velocity of computational node. For static-cartesian grid, the nodal velocity $\vec{v}$ becomes zero and Eulerain form of momentum (Eq.20) is achieved (Takashi and Hughes (1992)). Time discretization of flow equations is carried out by Chorin algorithm (Chorin (1973)) using pressure projection method which provides the velocity-pressure decoupling. The viscous term is treated with Crank-Nicholson scheme as used by Kim and Moin (1985), while convective term of momentum equation is dealt with Adam-Bashforth scheme. For the meshfree nodes RBF Finite Difference (RBF-FD) method is used to calculate spatial derivatives over random data points. Further details of the cartesian-meshfree hybrid zone have been discussed in detail by Javed *et al*. (2016), Javed *et al*. (2018) and Javed *et al*. (2019).

4.2 Fluid-Structure Coupling Scheme

The fluid-solid coupling has been achieved by a partitioned method; where close coupling at fluid-solid interface is achieved by solution of fluid and structural solvers iteratively at a single time step. The sub-iteration continues once the convergence between fluid and solid solvers is achieved before moving to the next time step. During sub iterations, the results are updated only over the meshfree zone to get fluid forces. The coupling algorithm proceeds where initially structural displacement S^{n+1} is calculated at time t^{n+1} based on the velocity and acceleration of previous time step t^n. The airfoil along with the whole meshfree cloud moves according to the predicted displacement S^{n+1}. The fluid equations are solved in accordance with the predicted structural displacement and updated fluid forces W^{n+1*} are calculated at the solid surface. The effective applied loads are calculated by aver-aging the fluid forces W^{n+1*} and W^n. The corrected structural deflection Sn+1 is achieved by solution of the structural equations which is compared with the corresponding value at the previous time step. The process continues until the structural displacement S^{n+1} achieves the desired convergence.

4.3 Validation of Proposed Scheme

To validate the solution scheme, same technique was applied to the semi-active flapping foil sys-tem in simple configuration and compared to Deng *et al.* (2015) solutions. Time varying pitch amplitude is given as $\theta(t) = \theta_o \sin(\omega t)$ while the heave amplitude is calculated from Eq.8. Mechanical, geometric and kinematic parameters are based on the tests conducted by Deng *et al.* (2015), where $k = 0$, $c = \pi$, $m = 0.1022$, $\theta_o = 75^o$, while foil is pitched at 13 of chord length. Simulations are conducted on

NACA0015 foil at *Re* = 1000 at two distinct non-dimensional frequencies (f^* = 0.12 and 0.16) while time variation of vertical force coefficient C_L during one period cycle is compared with those predicted by Deng *et al*. (2015). As shown in Fig.7, both results are in close agreement with each other while maximum lift coefficients achieved during the simulation are close to the already known results. It is also noted that peak value for the lift coefficient has increased with increment in non-dimensional frequencies, a trend which is also predicted by Deng *et al*. (2015).

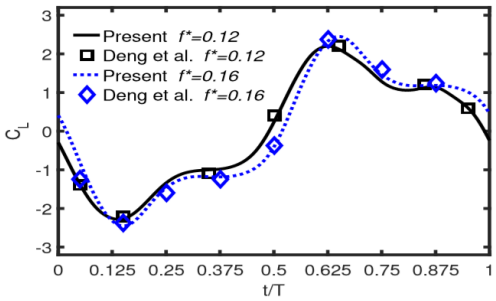

Fig.7. Calculated time variations of lift coefficient (C_L) over a period cycle for f^* = 0.12 and 0.16, k = 0, $c = \pi$, m = 0.1022 at θ0 = 75^o and *Re* = 1000. The results are in close agreement with Deng *et al*. (2015).

4.4 Prediction of Performance Parameters

Section 3. has predicted best performance for a coupled electromechanical system at some mechanical and kinematic parameters including k = 0, $c = 2\pi\rho bU$, m = 1 and $R = \frac{1}{C_p\omega}$. However, the analysis was based on Theodorsen thin-plate potential flow model which assumes low pitch amplitudes and small heaving frequencies. So, to cater for the viscous effects, numerical analysis has been carried out at the same optimal parameters. However, in-stead of thin plate, NACA 0015 foil at *Re* = 1100 is utilized where best performance has been indicated by Kinsey and Dumas (2008) and Deng *et al*.(2015) in their respective fully-active and semi-active flapping foil system analysis.

Simulations are conducted at five distinct pitch amplitudes θ_o = 15^o,20^o,60^o,76^o,85^o at pitch axis location of $a = -1/6$ corresponding to 1/3 of chord. The effect of varying reduced frequencies on the performance efficiency is examined as shown in Fig.8. It is worth mentioning that here another factor, cycle-averaged coefficient of power is defined at Eq.22 as:

$$\bar{C}_{op} = \frac{1}{T}\int_0^T C_{op}dt \tag{22}$$

where C_{op} is expressed as

$$C_{op} = \frac{P_{net}}{\frac{1}{2}\rho U_\infty^3 (2b)} \tag{23}$$

Here 2b represents the total chord length. Similar to Section 2., two type of efficiencies are defined; one based on total net power extracted through the flow η_{flow} (Eq.24) which includes the useful power extracted via piezoelectric transducer as well as damper which is also idealized as a power generator, while the other type of power is based on the net average electric power generated $\eta_{electric}$ (Eq.25). Average electric power is calculated based on Root Mean Square (RMS) value of generated voltage V_{rms}.

$$\eta_{flow} = \left(\bar{C}_{op}\right)_{flow}\frac{2b}{d} \tag{24}$$

$$\eta_{electric} = \left(\bar{C}_{op}\right)_{electric}\frac{2b}{d} \tag{25}$$

where d is the total vertical displacement of foil.

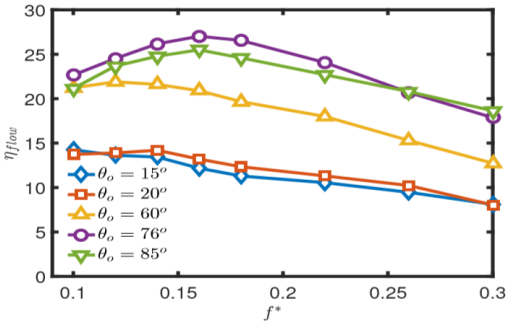

(a)

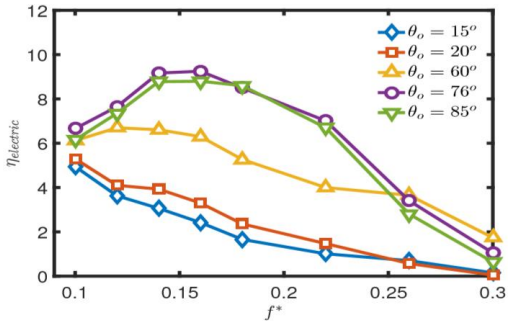

(b)

Fig. 8. Variation of (a) net harvested power efficiency(η_{flow}) and (b) net electric power efficiency($\eta_{electric}$) with reduce frequency at different pitch amplitudes (k = 0, $c = \pi$, *Re* = 1100). Maximum harvesting efficiency of η_{flow} = 27%and $\eta_{electric}$ = 9.2% is achieved at θ_o = 76^o.

From Fig. 8(a), it is observed that predicted efficiencies for pitch amplitudes of θ_o = 15^o,20^o and 60^o are low and decrease almost linearly with increment in reduced frequencies. However, the performance has improved for θ_o = 76^o and 85^o where there is an increment of efficiencies up to f^* = 0.16 and decrease there on. The maximum harvesting efficiency of η_{flow} = 27% is achieved at θ_o = 76^o and non-dimensional frequency of f^* = 0.16. This is less than η = 34%, the highest efficiency predicted by Deng *et al*. (2015) at θ_o = 75^o, f^* = 0.16 and *Re* = 1000. This is attributed to the fact that in present

case, we are dealing with a coupled electromechanical system where an electric transducer is coupled with a semi-active flapping foil system. Dynamics of the problem are now different and the power losses due to electric converter along with its associated efficiency is an important factor in reducing the efficiencies for the electromechanical systems when compared with known results from literature for fully and semi-active systems.

Figure 8(b) depicts the variation of average net electric power efficiencies $\eta_{electric}$ relation with respect to varying reduce frequencies where best performance ($\eta_{electric}$ = 9.2%) is achieved at $\theta_o = 76^o$ and $f^* = 0.16$. So out of the 27% power efficiency achieved from flow by the harvester, only 9.2% efficiency is based on useful electric power. Similar to case at Section 5., useful electric power efficiencies are low as compared to total energy extracted through the harvester which are attributed to energy loss due to conversion of the mechanical energy to electrical energy.

4.5 Dynamic Stall Effect

The evolution and shedding of LEVs are examined at two different pitch amplitudes $\theta_0 = 20^o$ (where effects of LEVs are minimal) and 76^o (where best harvester performance is achieved). The tests are performed at reduce frequency of $f^* = 0.16$ and $Re = 1100$ while other parameters are kept same. Figures 9 and 10 show the vortex topology for one time period cycle at $\theta_0 = 20^o$ and 76^o while Fig. 11 and Fig. 12 depicts the variation of prescribed pitching motion and hydrodynamic lift coefficient for one time period respectively. It is assumed that motion starts while foil is in pitch up motion at $t = T/8$. For $\theta_0 = 76^o$, the flow remains mostly attached for $t < T/8$, while the lift increases with increasing pitch angle and peak lift is achieved around $t = T/8$. Between $T/8 < t < T/4$, further increase in pitch angle results in flow separation from the foil's surface due to which there is reduction in lift as shown in Fig.12. During time interval $T/4 < t < 3T/8$, the leading edge vortex travels downstream along the surface and reattaches at the trailing edge which delays the stall due to low un-steady pitching rate resulting in slight increment in lift at $t = 3T/8$. With further decrease in pitch angle, the vortex leaves the trailing edge at $t = T/2$, resulting in the reduction of lift. The lift curve follows the same pattern in negative direction for the next half cycle.

For $\theta_0 = 20^o$, the flow has a tendency of separating from foil's leading edge due to low Reynolds number. Due to dominant viscous forces coupled with relatively low pitch angle and effective angle of at-tack, this flow does not reattach at the trailing edge as observed for $\theta_0 = 76^o$. So the lift coefficient is low as depicted for one time period cycle in Fig. 12.

To ascertain the effect of optimal timing of LEVs with the foil's motion, variation of coefficient of power $\bar{C}_{op}$, pitching moment C_M and pitching rate $\frac{d\theta(t)}{dt}$ is plotted over one time period cycle as shown in Fig.13. At $t < T/8$ the foil is in clockwise rotation while pitching rate and induced pitching moment have opposite signs. As power input is $P_{input} = M.\dot{\theta}$, so energy will be provided from the flow to foil and time average power coefficient ~~in-creases.~~ At $t > T/4$ the foil is in counter-clock wise rotation, while there is formation of LEVs that start traveling along the foil's surface towards trailing edge. The LEVs are low pressure region and as pitch axis is located at ~~13~~ of chord, this low pressure region at the trailing edge will produce a clockwise moment. Now both the pitch rate and pitch moment have same signs, so all this will result in energy transfer from foil to flow and the net power decreases. During the next quarter cycle $T/2 < t < 5T/8$, the foil is still in counter-clockwise rotation while pitching moment and rotation rates have opposite signs which entail energy transfer from flow to the foil, consequently increasing the net power coefficient. In this way, the energy is transferred between foil and the flow depending upon the foil's motion, induce pitching moment and LEVs formation.

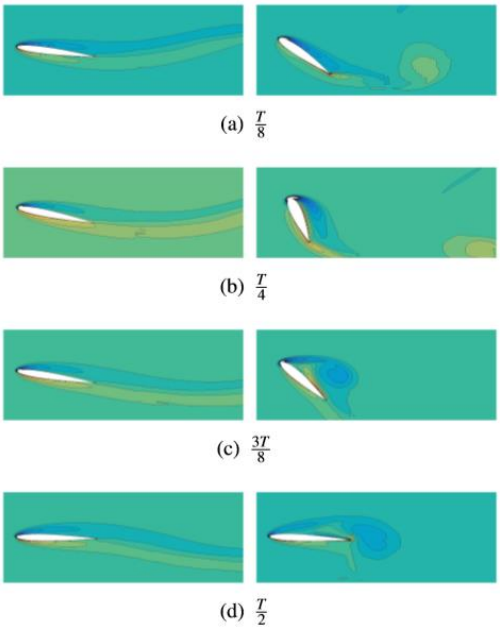

Fig. 9. Vortex evolution over half cycle i.e $0 < t < \frac{T}{2}$ for pitch amplitude $\theta_o = 20^o$ (left column) and 76^o (right column).

Figure 15 compares the efficiencies calculated through potential flow Theodorsen's model and numerical analysis based on RBF-FD meshfree solver. As discussed at Section 3.2, the threshold pitch amplitude of $\theta_0 = 20^o$ gives the best performance for harvested efficiencies when calculated through Theodorsen's thin-plate theory. Pitch amplitudes beyond 20o would result in flow separation violating the assumptions of Theodorsen's model. Same has also been studied physically in vortex plots at Fig. 9 and 10. Furthermore, analysis based on Theodorsen's model provides the optimum parameters where best performance is achieved. Same parameters have

been utilized during numerical analysis at Section 4., where maximum harvesting efficiency η_{flow} = 27% is achieved at θ_o = 76^o. So, it has been shown that harvesting performance has enhanced due to optimum utilization of dynamic stall effect.

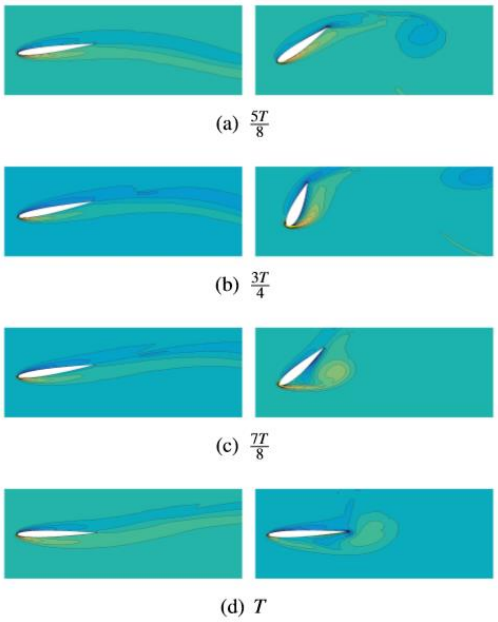

Fig. 10. Vortex evolution for other half cycle i.e. $\frac{T}{2} < t < T$ for pitch amplitude θ_o = 20^o (left column) and 76^o (right column).

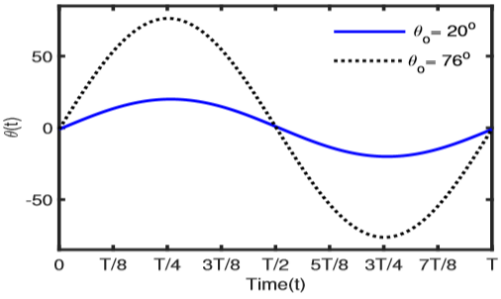

Fig. 11. Calculated variation of pitch amplitudes (θ_0 = 20^o and 76^o) over a period cycle for f^* = 0.16, k = 0, c = π, m = 1 and Re = 1100.

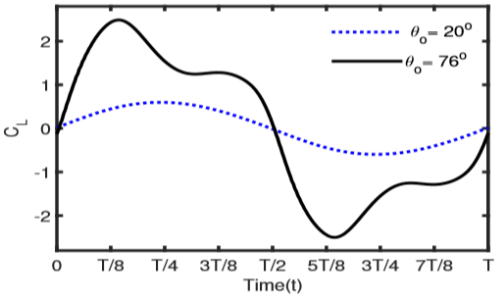

Fig. 12. Calculated variation of lift coefficient (C_L) over a period cycle for f^* = 0.16, k = 0, c = π, m = 1, Re = 1100 at θ_0 = 20^o and 76^o.

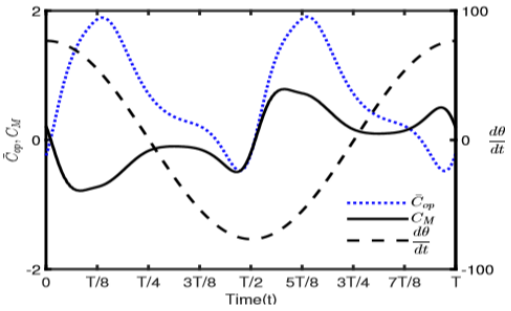

Fig. 13. Calculated variation of power coefficient $\bar{C}_{op}$, pitching moment C_M and pitching rate $\frac{d\theta(t)}{dt}$ over a period cycle for f^* = 0.16, k = 0, c = π, m = 1, Re = 1100 at θ_0 = 76^o.

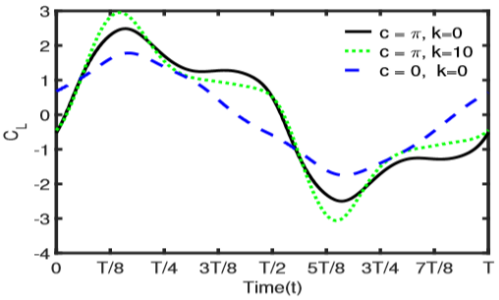

Fig. 14. Calculated variation of lift coefficient (C_L) over a period cycle for f^* = 0.16, m = 1, Re = 1100 at θ_0 = 76^o for different combinations of damping and stiffness.

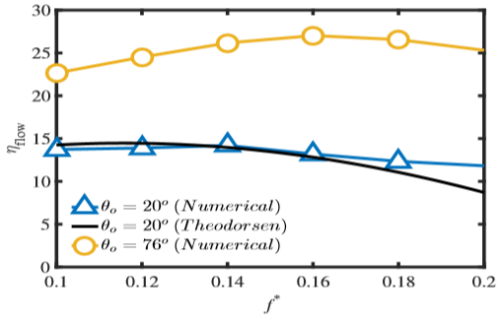

Fig. 15. Comparison of variation in net harvested power efficiency (η_{flow}) with reduced frequency (f^*) for Theodorsen [k = 0, c = π, a = −0.16 (31 of chord)] and Numerical [k = 0, c = π, a = −0.16 (13 of chord), Re = 1100] results.

4.6 Effect of Varying Stiffness and Damping

As shown before, the best performance is achieved at f^* = 0.16, θ_o = 76^o, Re = 1100 while optimized values of damping c = π and stiffness k = 0 are adopted based on our potential flow analysis and previous literature. However, to ascertain the effect of increased stiffness and zero damping strength, performance is compared at three different combinations of k and c while other parameters are kept constant unless stated otherwise. Firstly at c = π

Table 1 Comparison of RMS value of lift coefficient $(C_L)_{rms}$, maximum value of lift coefficient $(C_L)_{max}$, coefficient of net power output $\bar{C}_{op}$, vertical extent of foil d and efficiency η_{flow} at different combinations of stiffness and damping strength

Parameters $f^* = 0.16$, $m = 1$, $Re = 1100$, $\theta_0 = 76^o$	$(C_L)_{rms}$	$(C_L)_{max}$	$\bar{C}_{op}$	d	η_{flow}
$c = \pi$ and $k = 0$	1.60	2.49	0.47	1.75	0.27
$c = \pi$ and $k = 10$	1.64	2.95	0.24	1.01	0.24
$c = 0$ and $k = 0$	1.14	1.78	0.76	3.63	0.21

and $k = 0$, where the best performance is achieved; secondly at $c = \pi$ and $k = 10$ to determine the effect of increased stiffness and thirdly at $c = 0$ and $k = 0$ to examine the effect of zero damping. Figure 14 depicts the time variation of vertical force co-efficient at three different combinations of stiffness and damper strength. Similarly, Table 1 compares the RMS and maximum values of lift coefficient as well the power output and efficiencies at these three combinations. With increased stiffness ($k = 10$), both the maximum $(C_L)_{max}$ and $(C_L)_{rms}$ values for lift coefficient have increased when compared with ($k = 0$), which shows that vertical force coefficient is sensitive to k. The difference in coefficient of power $\bar{C}_{op}$ is significant for the two cases, where higher net power output is achieved at $k = 0$ coupled with higher vertical displacement d due to which the difference between the corresponding efficiencies for the two cases is not big enough. Such trend is also established by Wu *et al.* (2014) based on similar analysis.

With $k = 0$ established as the optimal stiffness, case for zero damping $c = 0$ along with $k = 0$ is investigated. It is observed that maximum and RMS values for lift coefficient $(C_L)_{max}$ and $(C_L)_{rms}$ respectively, have decreased compared with the optimal case for $k = 0$ & $c = \pi$. The coefficient of power $\bar{C}_{op}$ is higher than the previous two cases considered, however due to very large vertical displacement for the foil, the net efficiency based on total power extracted through the flow is less than the other two cases. This shows that there is always a particular value for damper which is associated with maximum performance of energy harvester.

5. CONCLUSION

Linearized coupled electromechanical equations have been used for piezoelectric energy harvesting through semi-active flapping foil system to fine-tune the values of various kinematic and mechanical parameters before conducting the computationally intensive Fluid-Structure-Interaction simulations. The aim is to maximize the piezoelectric power extraction and efficiency. Parametric analysis based on Theodorsen's thin plate model has revealed that net power output and efficiency are maximized when the foil is pitched at the mid-chord, stiffness is kept minimum at $k = 0$ and the damper strength of $c = 2\pi\rho bU$ based on flow conditions is utilized. Results are found to be affected by assumptions of potential flow and small amplitude motions inherent in the Theodorsen's model. However, threshold pitch amplitude of $\theta_o \approx 20^o$ is found to give the best estimate of performance where dynamic stall effects are negligible. More-over, an optimal value of piezoelectric resistance ($R_{opt} = \frac{1}{\omega C_p}$) is adopted for analysis which depends upon the capacitance of transducer as well as the forcing frequency. Two types of power outputs are defined, one through a piezoelectric transducer and the other through a combination of transducer and damper which is idealized as a power generator. The maximum efficiency through the electric converter is found to be 5% with power extraction of $0.37P_{max}$ around $\omega \approx 0.32$ rad/sec. The maximum power efficiency through the flow is 14% with corresponding power output of $0.56P_{max}$ at $\omega \approx 0.74$ rad/sec.

Analysis based on dynamic stall model revealed the best performance at pitch amplitude of $\theta_o = 76^o$ and non-dimensional frequency of $f^* = 0.16$ at $Re = 1100$. The maximum net power output efficiency through electric converter is found to be $\eta_{electric} = 9.2\%$ whereas maximum efficiency based on power output from flow is $\eta_{flow} = 27\%$. The power extraction efficiency η_{flow} is low com-pared to previously predicted results in literature, primarily due to mechanical-electric energy conversion between coupled electromechanical devices. The analysis of vortex generation, evolution, dissipation along with the hydrodynamic lift coefficients has depicted a strong association between the two, where net power output is strongly effected due to synchronization between pitch motion and induced pitching moment. Additionally, at low pitch angles the effect of LEVs is not dominant which results in low lift coefficients. The cases regarding spring with high stiffness and/or zero damping have resulted in reduction of

performance for the coupled electromechanical flapping foil energy harvester system, so such cases are not pursued further.

Incorporation of three dimensional effects caused by vortex dynamics would result in more accurate modeling of the problem and is suggested for future studies. Moreover, various other aspects including non-sinusoidal pitching motion, corrugated foils, multi-foil configuration and electric converters efficiencies may also be explored for an in-depth understanding of the subject.

REFERENCES

Abdelkefi, A., A. H. Nayfeh and M. Hajj (2012). Modeling and analysis of piezoaeroelastic energy harvesters. *Nonlinear Dynamics* 67(2), 925–939.

Anderson, J., K. Streitlien, D. Barrett and M. Triantafyllou (1998). Oscillating foils of high propulsive efficiency. *Journal of Fluid Mechanics* 360, 41–72.

Chin, W. K., Z. C. Ong, K. K. Kong, S. Y. Khoo, Y. H. Huang and W. T. Chong (2017). Enhancement of energy harvesting performance by a coupled bluff splitter body and pveh plate through vortex induced vibration near resonance. *Applied Sciences* 7(9), 921.

Chorin, A. J. (1973). Numerical study of slightly viscous flow. *Journal of fluid mechanics* 57(4), 785–796.

Deng, J., L. Teng, D. Pan and X. Shao (2015). Inertial effects of the semi-passive flap-ping foil on its energy extraction efficiency. *Physics of Fluids* 27(5), 053103.

Finnigan, T. D. (2012, October 16). Device for capturing energy from a fluid flow. *US Patent* 8,288,883.

Harper, K. A., M. D. Berkemeier and S. Grace (1998). Modeling the dynamics of spring-driven oscillating-foil propulsion. *IEEE Journal of Oceanic Engineering* 23(3), 285–296.

Hodges, D. H. and G. A. Pierce (2011). *Introduction to structural dynamics and aeroelasticity*, Volume 15. cambridge university press.

Jamil, M. and A. Javed (2019). Design optimization of a semi-active flapping foil in an energy extraction mode. In 2019 *International Conference on Engineering and Emerging Technologies (ICEET)*, 1–8. IEEE.

Javed, A., A. A. Baig, K. Djidjeli, A. Shahzad and A. Hameed (2019). Upwind skewed radial basis functions (usrbf) for solution of highly convective problems over meshfree nodes. *Engineering with Computers*, 1–17.

Javed, A., K. Djidjeli, A. Naveed, and J. Xing (2018). Low reynolds number effect on energy extraction performance of semi-passive flapping foil. *Journal of Applied Fluid Mechanics* 11(6) 1613-1627.

Javed, A., K. Djijdeli and J. Xing (2016). A coupled meshfree-mesh-based solution scheme on hybrid grid for flow-induced vibrations. *Acta Mechanica* 227(8), 2245–2274.

Javed, A., T. A. Shams, M. Bilal and M. Jameel (2018). Performance analysis of flapping foil flow energy harvester subjected to non-sinusoidal pitching motion. *In 2018 IEEE 21st International Multi-Topic Conference* (INMIC), pp. 1–5. IEEE.

Kim, J. and P. Moin (1985). Application of a fractional-step method to incompressible navier-stokes equations. *Journal of computational physics* 59(2), 308–323.

Kinsey, T. and G. Dumas (2008). Parametric study of an oscillating airfoil in a power-extraction regime. *AIAA journal* 46(6), 1318–1330.

Kinsey, T. and G. Dumas (2014). Optimal operating parameters for an oscillating foil turbine at reynolds number 500,000. *AIAA Journal* 52(9), 1885–1895.

Mehmood, A., A. Abdelkefi, M. Hajj, A. Nayfeh, I. Akhtar and A. Nuhait (2013). Piezoelectric energy harvesting from vortex-induced vibrations of circular cylinder. *Journal of Sound and Vibration* 332(19), 4656–4667.

Qadri, M. M., A. Shahzad, F. Zhao and H. Tang (2019). An experimental investigation of a passively flapping foil in energy harvesting mode. *Journal of Applied Fluid Mechanics* 12(5), 1547–1561.

Shimizu, E., K. Isogai and S. Obayashi (2008). Multiobjective design study of a flapping wing power generator. *Journal of Fluids Engineering* 130(2), 021104.

Shyy, W., H. Aono, S. K. Chimakurthi, P. Trizila, C. K. Kang, C. E. Cesnik and H. Liu (2010). Recent progress in flapping wing aerodynamics and aeroelasticity. *Progress in Aerospace Sciences* 46(7), 284–327.

Takashi, N. and T. J. Hughes (1992). An arbitrary lagrangianeulerian finite element method for interaction of fluid and a rigid body. *Computer methods in applied mechanics and engineering* 95(1), 115–138.

Triantafyllou, M. S., A. H. Techet and F. S. Hover (2004). Review of experimental work in biomimetic foils. *IEEE Journal of Oceanic Engineering* 29(3), 585–594.

Wu, J., Y. Chen, N. Zhao and T. Wang (2016). Influence of stroke deviation on the power extraction performance of a fully-active flap-ping foil. *Renewable Energy* 94, 440–451.

Wu, J., Y. Qiu, C. Shu,and N. Zhao (2014). Pitching-motion-activated flapping foil near solid walls for power extraction: A numerical investigation. *Physics of Fluids* 26(8), 083601.

Xiao, Q., W. Liao, S. Yang and Y. Peng (2012). How motion trajectory affects energy extraction

performance of a biomimic energy generator with an oscillating foil? *Renewable Energy* 37(1), 61–75.

Xiao, Q. and Q. Zhu (2014). A review on flow energy harvesters based on flapping foils. *Journal of fluids and structures* 46, 174–191.

Zhu, Q. (2011). Optimal frequency for flow energy harvesting of a flapping foil. *Journal of fluid mechanics* 675, 495–517.

Zhu, Q., M. Haase and C. H. Wu (2009). Modeling the capacity of a novel flow-energy harvester. *Applied Mathematical Modelling* 33(5), 2207–2217.

Zhu, Q. and Z. Peng (2009). Mode coupling and flow energy harvesting by a flapping foil. *Physics of Fluids* 21(3), 033601.